Journal of Physics: Conference Series

PAPER • OPEN ACCESS

Experimental investigation of electrically enhanced boiling of FC 72 using high-resolution phase-detection diagnostics

To cite this article: Marco Graffiedi *et al* 2024 *J. Phys.: Conf. Ser.* **2766** 012140

View the article online for updates and enhancements.

You may also like

- The Effect of Mass Flow Rate and Heat Flux on Vertical Two-Phase Flow Regimes in a Small Diameter Tube
Ali K. Mohammed, Majid H. Majeed and Ahmed Q. Mohammed
- Properties of Movement and Boiling of Speckles Produced by Moving Objects Illuminated with Partially Coherent Light
Teng Shu-Yun, Cheng Chuan-Fu, Liu Man et al.
- Numerical hybrid thermal MRT-LBM for condensation and boiling phenomena on horizontal walls of different wettability
Salaheddine Channouf, Mohammed Jami and Ahmed Mezrhab

This content was downloaded from IP address 131.114.71.212 on 27/08/2024 at 08:43

Journal of Physics: Conference Series **2766** (2024) 012140 doi:10.1088/1742-6596/2766/1/012140

Experimental investigation of electrically enhanced boiling of FC 72 using high-resolution phase-detection diagnostics

Marco Graffiedi[1], Alekos Ioannis Garivalis[2], Paolo Di Marco[2] and Matteo Bucci[1]
[1] Nuclear Science and Engineering, Massachusetts Institute of Technology, Cambridge 02139, US

[2] Department of Energy, Systems, Territory and Constructions Engineering, University of Pisa, Largo Lucio Lazzarino, 56122 Pisa, Italy

E-mail: mgraff@mit.edu

Abstract. This work features the boiling of FC72 on a transparent sapphire substrate. Tests are performed using a thin ITO film (indium tin oxide) coated on the sapphire substrate as the heat source, a fast speed video camera to capture the boiling process using a technique to track the phase (liquid or vapor) in contact with the heating surface, an InfraRed video camera to capture the average temperature on the surface, and a metallic grid to impose an electric field perpendicular to the boiling surface. The maximum average electric field tested in this work is $3.3 kV/mm$, which led to a 18% increase of the critical heat flux. This study analyses in detail the phase distribution data showing that (1) there is no evidence of microlayer formation, and suggesting that (2) the triple contact line evaporation accounts for approximately 20% of the total heat flux, while (3) the quenching stage accounts for approximately 80%. Finally, phase distribution images are processed to characterize the size of vapor patches, showing that a boiling crisis occurs when the distribution of the vapor patches becomes scale-free, and corroborating the hypothesis that the boiling crisis can be modelled as a bubble interaction instability using a percolation model.

1. Introduction

With the surge in electric transportation and the exponential growth of computing power, there is a compelling need for increasingly efficient and compact cooling systems. Within the realm of electronic cooling, liquid cooling is gaining prominence over air cooling due to its enhanced consistency and efficiency. For instance, single-phase and two-phase thermal control systems have been proposed for cooling power electronics and battery packs in the automotive industry [1]. Immersion cooling relies on natural convection to remove heat especially when two phase heat transfer is used. Direct cooling has also been proposed for electronic cooling in space applications [2-3]. However, the lack of natural recirculation in microgravity environments requires other external actions to move the fluid, such as pumps or the use of high intensity electric fields (EF) which enhance bubbles detachment from the surface in boiling heat transfer [4].

In this work, we discuss the results of an experimental investigation focused on elucidating the effect of EFs on the boiling dynamics and the CHF limits of a dielectric fluid, FC-72 (C_6F_{14}), manufactured by 3M and often used for direct cooling of electronic components. To this end, we developed an experimental setup that enables the use of advanced optical diagnostic to track the time-dependent distributions of the liquid and vapor phase in contact with the heating surface. Thank to this diagnostics,

Content from this work may be used under the terms of the Creative Commons Attribution 4.0 licence. Any further distribution of this work must maintain attribution to the author(s) and the title of the work, journal citation and DOI.
Published under licence by IOP Publishing Ltd

we can shed light on the mechanism of heat transfer during the boiling of FC-72 as well as the mechanisms triggering a departure from nucleate boiling.

2. Experimental apparatus

The apparatus, shown in figure 1, is built around a $1mm$ thick, $20 \times 20\ mm^2$ wide sapphire substrate. The heating element is a $700\ nm$ indium tin oxide (ITO) film coated on top of the sapphire substrate, which can be electrically heated. The electric power sent to the ITO is calculated by measuring the voltage at the heater pads and knowing the resistance of the ITO film, which was measured separately with high precision. Regarding the heat flux determination, the power is considered homogeneously distributed on the $10 \times 10\ mm^2$ ITO surface. The sapphire is assembled in a 3D printed resin cartridge featuring a stainless-steel plate aligned with the ITO and a stainless-steel grid $6\ mm$ above the ITO. Using a high voltage power supply, we impose a positive voltage on the grid while grounding the ITO heater and the stainless-steel plate. During the tests the high voltage power supply was used to impose a positive d.c. voltage on the grid up to $20\ kV$.

The sapphire surface is recorded using 2 cameras simultaneously. A high-speed camera is used to image the ITO surface from the bottom with a 20° incident angle. The surface is lighted by a coherent LED light with a 20° incident angle in such a way that the phase detection technique can be used. In particular, this technique permits to detect microlayers with a thickness up to $10\ \mu m$ [5]. The infrared camera is used to image the sapphire from the bottom and measure the temperature on the surface.

The IR measurements during the boiling process were characterized by an appreciable variation of temperature along the surface and very little difference in temperature between dry and wet areas. The former leads the accuracy in the measurement of the average temperature of the surface, which can go from a minimum of $\pm 2°C$ to a maximum of $\pm 5°C$. The latter creates difficulties in determining the heat flux between the solid and the liquid. This small temperature sensitivity to the boiling process is in accordance with another work featuring boiling of FC72 on sapphire [6], due to the high thermal diffusivity of sapphire. In conclusion, the IR video will not be used to calculate the time-dependent distribution of heat flux between the surface and the liquid, but only to measure the average surface temperature.

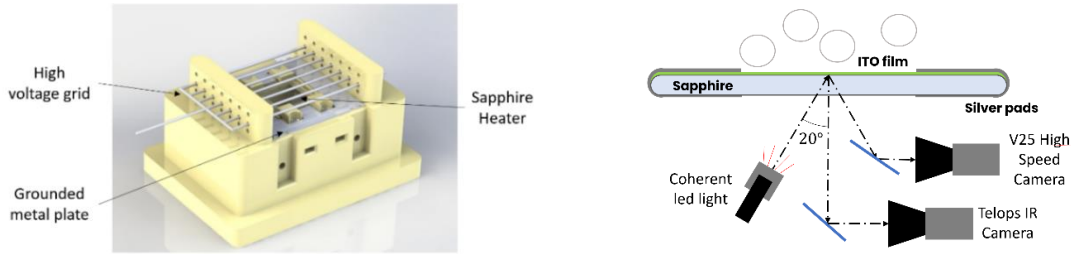

Figure 1. On the left, Cartridge schematic; on the right, the detail of the sapphire heater and the cameras used in the experiment.

3. Results

3.1. Boiling curves

All boiling curves are performed at a pressure of $101 \pm 5kPa$ and a corresponding saturation temperature of $T_b = 56°C$. The tests are conducted with $0kV$, $10kV$, $15kV$, and $20kV$ of potential between the grid and the heater. The resulting boiling curves are reported and compared with different other studies in figure 2. As it can be seen, the critical heat flux increases of 25% between the case without electric field and with $20kV$ of imposed voltage.

3.2. Image segmentation and percolation theory

Starting from the high-speed video of the phase detection, we binarize the image and then detect and track vapor patches. The binarization of each image starts by removing the background from the image,

slightly blurring it, and correct for non-uniform illumination. Then, the Otsu's method is used to perform an automatic image thresholding. From this image processing, it is possible to calculate the dry area fraction (DAF) and the contact line density (CLD).

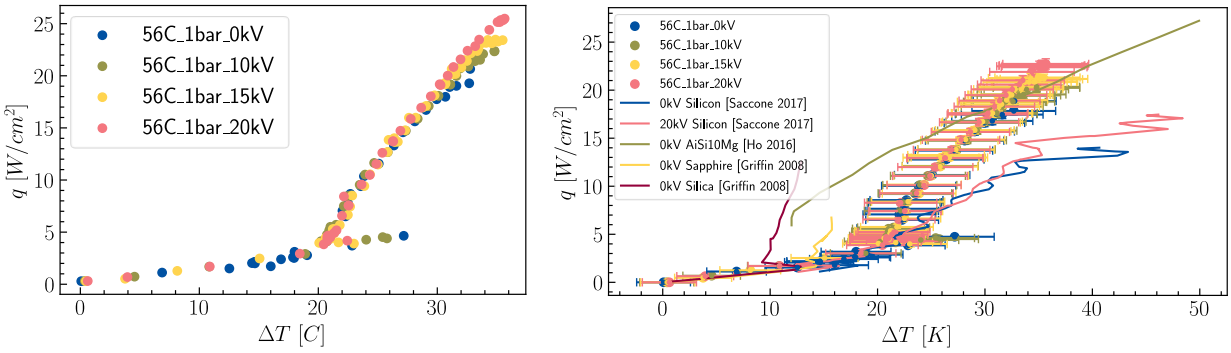

Figure 2. On the left, boiling curves in saturation conditions at 101 kPa with different voltage (i.e., EF) levels (these data are plotted without error bars). On the right, the same data are compared with boiling curves obtained in similar operating conditions by other authors.

As it can be seen from the DAF and CLF plots in figure 3, increasing the voltage level reduces the dry areas on the boiling surface. Moreover, it seems that the DAF has a maximum value at approximately 0.6. Conversely, the CLD seems to be unaffected by the voltage level. The electric field seems to reduce the size of the bubbles while increasing the number of bubbles on the surface. A deeper investigation can be made by analyzing the probability distribution of dry areas.

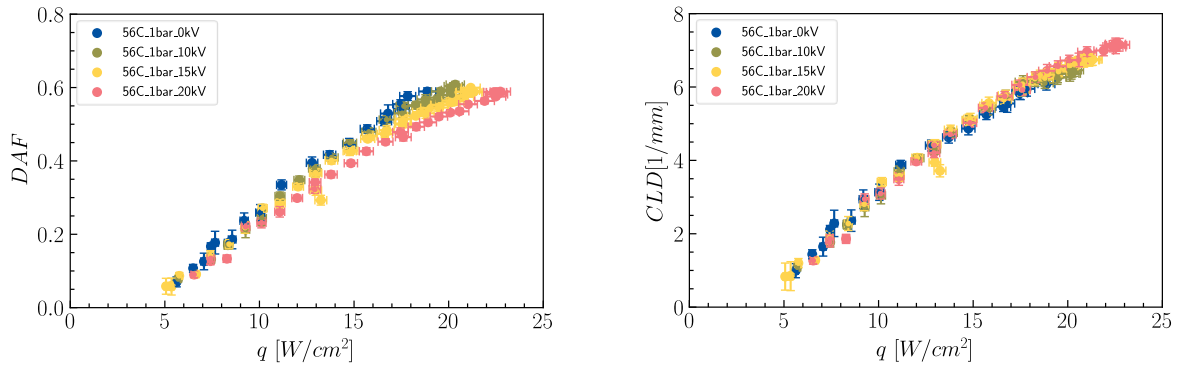

Figure 3. On the left, dry area fraction (DAF). On the right, contact line density (CLD). Both quantities are measured by post-processing the phase detection videos

Focusing on probability distribution of dry areas in figure 4, we can see that for low heat fluxes, the footprint area PDF decreases rapidly following an exponential decay. Approaching to the DNB, the distribution becomes a power law function $\boldsymbol{P(A) \approx A^{-\tau}}$, where $\tau = 2$ is the Fisher exponent. The power-law distribution with $\tau < 3$ indicates a scale free phenomenon, which is consistent with separate observations published in another study [7]. Curiously, the presence of high electric field delays the raise in DAF and the appearance of a power-law distribution. This suggests that bubbles have higher interaction probability (e.g., due to a larger bubble footprint radius) at low electric fields and lower interaction probability at higher electric fields. This is consistent with previous experiments that reported the tendency of bubbles to grow taller and narrower in the presence of electric fields [4,8]. Since the determination of the bubble shape is a non-trivial exercise, it will be the analyzed more in detail in a future work.

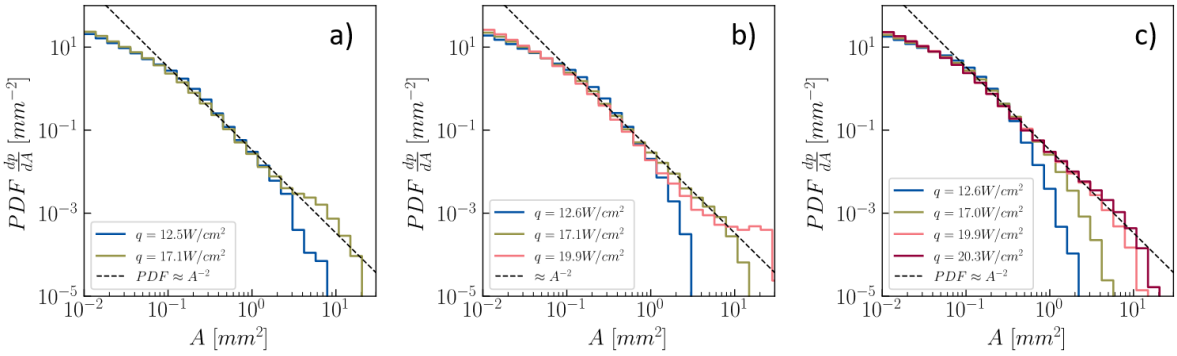

Figure 4. Probability density functions of dry areas, plotted for different heat flux level with a) 0kV/mm, b) 10kV/mm, and c) 20kV/mm electric field intensities.

3.3. Microlayer un-detection

In our operating conditions, Cooper model [9], as well as the criterion on the critical velocity proposed by Urbano [10] and the model on maximum critical radius by Bures [11] would predict the formation of a detectable microlayer. However, we did not observe any interference fringe indicating the presence of such microlayer in any of the test conducted. In conclusion, our observations are not in accordance with all the cited models. This calls for more investigations on the formation and evaporation of microlayer in different fluids.

4. Hypothesis and modelling

4.1. TCL evaporation

The static contact angle of FC-72 measured on smooth ITO is 11° [12]. When evaporation occurs, the apparent contact angle increases due to the liquid mass flow rate in the microregion near the TCL and the recoil from the liquid evaporation. In the present work, we will use the model proposed by Raj [13] to simulate the microregion. We choose this model because it has been validated on the evaporation of FC-72 droplets at ambient pressure. In our particular situation, we have neglected the impact of the electric field on the microregion. The assumption that the effect of the electric field can be neglected is consistent with the fact that the liquid in microlayer is electrically shielded by the overhead mass of vapor, and will be better validated in a future work. The contact angle and the TCL evaporation resulting from the model, calculated using the bubble base radius from the experiments, are represented in figure 5. Based on these results, we can estimate the contribution of the TCL evaporation on the overall heat flux as $q''_{TCL} = q'_{TCL} \times CLD$.

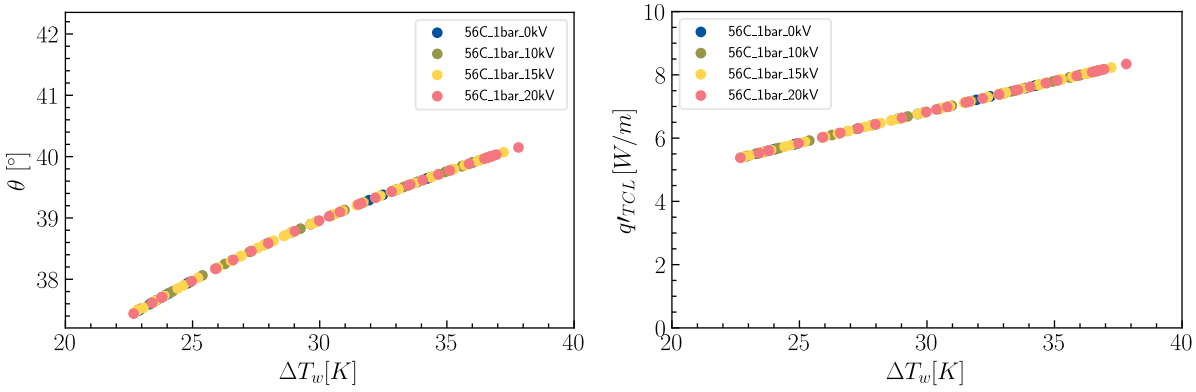

Figure 5. Left, Contact angle at different temperature; right, the triple contact line evaporation term at different temperature, according to [13].

4.2. Quenching

Considering that the effusivity of the sapphire is considerably larger than the effusivity of the fluid, it is reasonable to assume a constant wall temperature T_W during rewetting of the dry areas. If we consider the quenching to last for a time t_Q, the mean heat flux during quenching can be computed as $< q''_{qc} > = 2\varepsilon_l \frac{T_W - T_b}{\sqrt{\pi}\sqrt{t_Q}}$ [14]. We used the phase detection videos to track wet and dry areas. In particular we can determine, for each pixel, at which time the surface is wet or dry. With this information, we are able to compute the t_Q for every quenching event and compute the average quenching heat flux as $< q''_{qc} >$. Then, we can sum over all the quenching events (i) of every pixel (j) and average it in time:

$$\boldsymbol{q''_{qc} = \frac{1}{N_{pixel} t_{max}} \sum_i \sum_j < q''_{qc} >_{ij} t_{Q_{ij}}}$$

where t_{max} is the time span of the analyzed video and N_{pixel} is the number of pixel analyzed.

4.3. Comparison of TCL and Quenching with the experimental heat flux

The results from the previous formulation of q''_{qc} and q''_{TCL} are reported in figure 6. As it can be seen, the contribution of the TCL evaporation is fairly small and goes from 5-10% near the onset of nucleate boiling to almost 25% of the total heat flux near the boiling crisis. Instead, quenching heat transfer accounts for 70-80% of the total heat flux. The model tends to underpredict the heat transfer near the onset of nucleate boiling, this discrepancy is easily explained by considering that we are neglecting the contribution of the natural convection to the heat transfer. Instead, the model tends to overpredict the heat transfer near the boiling crisis, especially for high voltage levels. This might be explained by how the contact angle has been considered and calculated. As previously stated, the presence of electric field tends to "pull" upwards the bubbles increasing the contact angle, this effect is not considered in the model that we used to simulate the microregion near the TCL. If indeed we have a greater contact angle, this would reduce the TCL evaporation for high electric fields. The determination of the contact angle in high electric fields is a non-trivial exercise and will be the subject of a future work. However, as shown in figure 6, our mechanistic reconstruction of the boiling curve is fairly accurate.

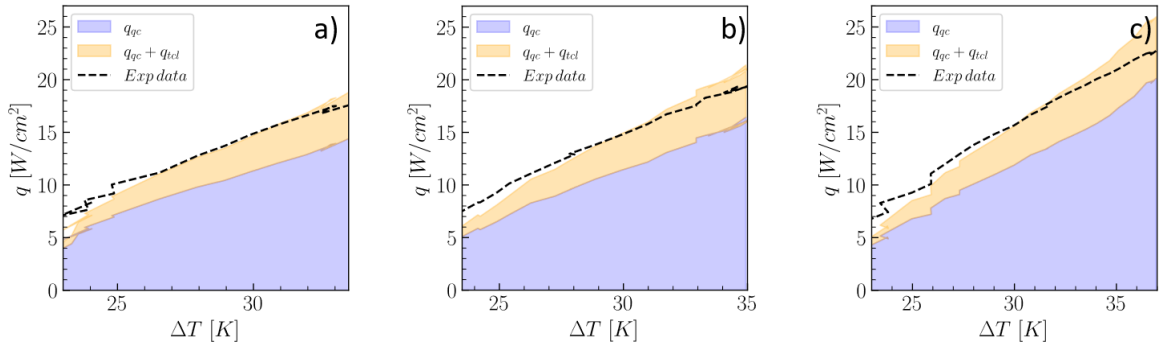

Figure 6. Boiling curves in the nucleate boiling regime with detail on the triple contact line evaporation and quenching for different electric potentials. a) 0kV/6mm, b) 10kV/6mm, and c) 20kV/6mm electric field intensities.

5. Conclusions

Although different models in literature predicts the formation of the microlayer when boiling FC-72, we shown that there is no evidence of microlayer formation, which indicates that the triple contact line evaporation accounts for almost all the evaporation term in the heat flux partitioning. This is consistent with the observations of other investigators [15]. We evaluated the contribution of the TCL evaporation and quenching mechanistically showing that they can account for almost all the heat transfer in the nucleate boiling regime. Finally, we have showed the signature of the boiling crisis in the power-law

probabilistic distribution of the bubble footprint areas. This observation corroborates previous findings, suggesting that a boiling crisis is triggered by an instability in the near-wall bubble interaction process. By comparing the dry area fraction distributions, we observe that by increasing the electric field at a given heat flux value, the bubble footprints get smaller, reducing the probability of interaction between bubbles. Thus, the value of the CHF at which a boiling crisis occurs increases when an EF is applied.

References

[1] Moreno G, Narumanchi S, Tomerlin J and Major J 2022 Single-phase dielectric fluid management for power-dense automotive power electronics, *IEEE Trans Power Electron* **37** 12474–85.
[2] Saccone G, Di Marco P, Bucci M, Moran JL and Buongiorno J 2017 Critical Heat Flux Enhancement in Presence of Microstructured Surfaces and Electric Field *9th World Conference on Experimental Heat Transfer, Fluid Mechanics and Thermodynamics* **12**
[3] Straub J, Picker G, Winter J and Zell M 1997 Effective cooling of electronic components by boiling phase transition in microgravity *Acta Astronaut* **40** 2–8
[4] Garivalis AI and Di Marco P 2022 Isolated bubbles growing and detaching within an electric field in microgravity *Appl Therm Eng* **212** 118538
[5] Kossolapov A, Phillips B and Bucci M 2021 Can LED lights replace lasers for detailed investigations of boiling phenomena *International Journal of Multiphase Flow* **135** 103522
[6] Griffin A 2008 Fundamental Study Of Fc-72 Pool Boiling Surface Temperature Fluctuations And Bubble Behavior PhD Thesis *University of Central Florida*
[7] Zhang L et al A 2023 unifying criterion of the boiling crisis *Nature Communications* **14** 1
[8] Ogata J and Yabe A 1993 Basic study on the enhancement of nucleate boiling heat transfer by applying electric fields *Int J Heat Mass Transf* **36** 3
[9] Cooper MG and Lloyd AJP 1969 The microlayer in nucleate pool boiling *Int J Heat Mass Transf* **12** 8
[10] Urbano A, Tanguy S, Huber G and Colin C 2018 Direct numerical simulation of nucleate boiling in micro-layer regime *Int J Heat Mass Transf* **123** 1128
[11] Bureš L and Sato Y 2021 On the modelling of the transition between contact-line and microlayer evaporation regimes in nucleate boiling *J Fluid Mech* **916** A53
[12] McHale JP and Garimella SV 2013 Nucleate boiling from smooth and rough surfaces – Part 1: Fabrication and characterization of an optically transparent heater–sensor substrate with controlled surface roughness *Exp Therm Fluid Sci* **44** 456–467
[13] Raj R, Kunkelmann C, Stephan P, Plawsky J and Kim J 2011 Contact line behavior for a highly wetting fluid under superheated conditions *Int J Heat Mass Transf* **55** 9–10
[14] Del Valle VH and Kenning DBR 1985 Subcooled flow boiling at high heat flux *Int J Heat Mass Transf* **28** 10
[15] Schweizer N, Di Marco P and Stephan P 2013 Investigation of wall temperature and heat flux distribution during nucleate boiling in the presence of an electric field and in variable gravity *Exp Therm Fluid Sci* **44** 419–430
[16] Ho JY, Wong KK and Leong KC 2016 Saturated pool boiling of FC-72 from enhanced surfaces produced by Selective Laser Melting *Int J Heat Mass Transf* **99** 107–121